

Role of pore-size distribution on effective rheology of two-phase flow in porous media

Subhadeep Roy^a, Santanu Sinha^{b,c}, Alex Hansen^b

^a*PoreLab, Department of Physics, University of Oslo, NO-0371 OSLO, Norway*

^b*PoreLab, Department of Physics, Norwegian University of Science and Technology, N-7491 Trondheim, Norway.*

^c*Beijing Computational Science Research Center, 10 East Xibeiwang Road, Haidian District, Beijing 100193, China.*

Abstract

The flow of immiscible fluids inside a porous medium shows non-linearity in the form of a power law in the rheological properties of the fluids under steady state flow conditions. However, different experimental and numerical studies have reported different values for the exponent related to this power law. Here we explore how the rheological properties of the two-phase flow in porous media depends on the distribution of the pore sizes and how it affects the power-law exponent. The pore-size distribution controls fluctuation in the pore radii and their density in a porous material. We present two approaches, analytical calculations using a capillary bundle model and numerical simulations using dynamic pore-network modeling. We observe crossover from a non-linear to linear rheology when increasing the flow rate where the non-linear part is highly affected by the pore-size distribution. We have also carried out the study for different saturations of the two fluids.

Keywords: non-linear fluid flow, two-phase flow, porous media

1. Introduction

Multiphase flow is relevant to a wide variety of different applications which deal with the flow of multiple immiscible fluids in single capillaries to more complex porous media [1, 2]. The rheology of such flow is guided by a series of parameters: capillary forces at the interfaces, viscosity contrast between the fluids, wettability and geometry of the system, which collectively make the flow properties different compared to single phase flow. The study of two-phase flow is generally divided in two regimes: (i) the transient regime and (ii) the steady-state flow. In the transient regime, one can obtain different types of flow patterns, namely capillary fingering [3], viscous fingering [4, 5] and stable displacement [6], and models such as diffusion limited aggregation (DLA) [7] and invasion percolation [8] are used to describe the patterns. When the steady state sets in after the initial instabilities, the flow properties are determined by the global parameters such as global pressure drops, flow rates, saturation and fractional flow [9].

In recent years, many studies on the steady-state two phase flow on Newtonian fluids have revealed a non-trivial rheology, that is, in the regime where capillary forces are comparable to viscous forces, the relation between the total flow rate Q in a sample and the global pressure drop ΔP across it differs from a linear Darcy law [10, 11]. Instead, Q increases much faster with ΔP , obeying a power law where the power-law exponent β is larger than 1 [12–15]. Furthermore, studies have also shown that it undergoes crossovers to linear regimes at both sides of the non-linear regime, that is, at flow rates below a threshold and at flow rates higher than another larger threshold. Experiments by Tallakstad et al. for a two-dimensional (2D) Hele-Shaw cell filled with glass beads measured this exponent β as 1.85 ($\approx 1/0.54$)¹ [12, 13]. For a three-dimensional (3D) porous media, this exponent was observed to

Email addresses: subhadeeproy03@gmail.com (Subhadeep Roy), santanu.sinha@ntnu.no (Santanu Sinha), alex.hansen@ntnu.no (Alex Hansen)

¹The values in the brackets are the exponents reported in the literature, the reciprocals of them should be compared here, as we express our results as Q as a power law in ΔP , whereas the cited articles expressed ΔP as a power law in Q , or rather the corresponding capillary number Ca .

vary between 2.2 ($\approx 1/0.45$) and 3.3 ($\approx 1/0.3$) [14] depending on the saturation. It was later found to converge to a certain value ≈ 2.17 when a global yield pressure is considered in the system, under which there is no flow [15]. By using pore-network modeling with 2D and 3D pore networks, Sinha et al. found the exponent to be close to 2 in the non-linear regime [15, 16]. They also have reported a crossover to linear Darcy type regime at high capillary number when capillary forces are insignificant. Yiotis et al. performed Lattice-Boltzmann simulations with stochastically reconstructed porous system and studied the dynamics of fluid blobs in the presence of gravity [17]. In the steady state, they found a non-linear regime with quadratic dependence with an exponent 2, which is bounded by two linear regimes at both the high and low capillary numbers. The blobs were then studied experimentally and the non-linear exponent was found as 1.54 ($\approx 1/0.65$) [18]. Very recently, Gao et al. performed experiments of two-phase flow in sandstone samples. They used x-ray micro-tomography measurements and for a fractional flow of 0.5 they found the exponent in the non-linear regime to be equal to 1.67 ($\approx 1/0.6$) [19]. They also reported a regime with linear Darcy type behavior at lower capillary numbers where the conductance does not change significantly. Further experiments by Zhang et al. [20] explore the dependence of the exponent on fractional flow and reported values in the range of 1.35 ($\approx 1/0.74$) to 2.27 ($\approx 1/0.44$). They presented a theory that can predict the boundary between the linear regime and the non-linear intermittent flow regime.

A simple explanation for the observed power law relation between flow rate and pressure drop may be found by following the arguments of Roux and Herrmann [21], concerning the conductivity of a disordered network of resistors, where each resistor has a threshold voltage to start conducting current. If we compare the voltage across a resistor in this system to the pressure drop over a link in a network of pores, and the threshold voltage to the pressure drop necessary to overcome capillary forces due to the presence of fluid interfaces [22], we may translate the Roux and Herrmann arguments into a language appropriate for porous media. When the pressure drop ΔP across a network of pores containing fluid interfaces is increased by an amount $d\Delta P$, an additional number of pores (dN) will start contributing to the flow. This leads to an increase in the effective conductivity of the network as more links are participating in the flow. If correlations between the opened links are ignored, the increase in conductivity will be proportional to the increase in the number of opened links, $dK \propto dN$. We integrate to find

$$K(\Delta P') \propto \int_{P_c}^{\Delta P'} d\Delta P'' = \Delta P' - P_c, \quad (1)$$

where the lower integration limit is determined by the threshold pressure necessary to overcome to induce flow across the network. The flow rate is then given by

$$Q = \int_{P_c}^{\Delta P} K(\Delta P') d\Delta P' \propto (\Delta P - P_c)^2. \quad (2)$$

Tallakstad et al. [12, 13] provided another explanation by considering the scaling of clusters that are trapped by capillary forces. They assumed that the flow occurs in channels in between trapped clusters. In a two-dimensional system of length L under a pressure drop ΔP , a cluster will be trapped if the capillary force $p_c > \lambda_{\parallel} |\Delta P|/L$, where the λ_{\parallel} is the length of such a cluster. The maximum length of a such a trapped cluster is therefore given by $\lambda_{\parallel}^m = L p_c / |\Delta P|$. By assuming the distance between the flow channels equal to the typical cluster length, the total number of flow channels will be $n_c = L / \lambda_{\parallel}^m$. The total flow through all the channels is therefore the number of channels multiplied by the flow rate in each channel, which leads to $Q \propto n_c |\Delta P| \propto |\Delta P|^2$. However, if this formalism is extended to three dimensions, it leads to a cubic relationship, $Q \propto |\Delta P|^3$, which is in contrary to what is observed in experiments and simulations.

Sinha and Hansen [16] developed a mean-field theory for a disordered network. By analytically calculating the average rheological behavior for such a pore [22] and using Kirkpatrick's self-consistent expression for the equivalent

conductivity for a homogeneous network [23], they derived the relationship,

$$Q \propto (\Delta P - P_c)^\beta. \quad (3)$$

Note that the above theoretical approaches find the exponent in the non-linear regime β to be equal to 2, thus hinting at universality.

Recently, Roy et al. have studied the effect of the threshold distribution on the effective rheology of two Newtonian fluids in a capillary bundle model [24]. The model consists of a bundle of parallel capillary tubes with variable diameters along their lengths which introduce thresholds for each tube [25, 26]. For power-law type distributions of the thresholds they find analytically and numerically that the non-linear exponent β can be related to α , the exponent for the power-law distribution, by the relationships $\beta = \alpha + 1$ or $\beta = \alpha + 1/2$ depending on whether the distribution starts from zero or has lower cut off respectively. This means, for $\alpha = 1$, the uniform threshold distribution, β will be equal to 2 and 3/2 respectively for the two cases. This study clearly hints at the non-linear exponent depends on the distributions related to the system properties. We note that the capillary fiber bundle model in the form studied by Roy et al. only considered variations in the flow thresholds and not directly on the variations in the pore sizes, nor fluctuations in the saturation.

In this article, we present a detailed study how the distribution of pore sizes controls the effective rheology of the two-phase flow in the steady state. We will first study analytically the capillary bundle model, as it is an analytically tractable model for two-phase flow and provides deeper understanding of the underlying physical mechanism. There we will show that there exists a transition point as the applied pressure is increased below which the relation between flow rate and pressure drop is non-linear. We will investigate how the degree of such non-linearity depends on the shape and the width of the distribution. Above the transition point we observe Darcy-like linear flow where the distribution of pore sizes do not have any affect on the flow equation. We will then move to numerical simulation with dynamic pore-network modeling, where the similar transition is observed. There the variation in exponent in the non-linear regime and the transition point is studied by varying three parameters: the saturation of the wetting fluid, and the span and shape related to the pore-size distribution. Finally, with a two-dimensional plane of the non-linear exponent vs the transition point, we show how the above three parameters control the effective rheology of two-phase flow.

2. Capillary Fiber Bundle Model

In this section, we will study the analytically solvable *capillary fiber bundle model* (CFBM) [25, 26], which is a prototype for a one-dimensional porous medium. The present authors have recently explored [24] this model in order to explore a transition from non-linear to a Darcy-like behavior when the pressure gradient across the system is continuously increased. CFBM is a hydrodynamic analog of the fiber bundle model [27], which is a disordered system driven by threshold activated dynamics and often used as a model system to study mechanical failure under stress.

The model consists of a bundle of N independent parallel tubes of length L , carrying train of bubbles with different distributions of wetting and non-wetting fluids. A global pressure drop ΔP is applied across the bundle, creating a global flow rate Q . In the steady state, Q is the sum of all the time averaged flow rates $\langle q \rangle$ in each individual tube. The diameter of each tube varies along the length of the tubes which makes the interfacial forces vary as the bubble train moves along the tubes. We assume no film flow so the fluids do not pass each other. The total length of the sections along the tube containing the more wetting fluid (called the wetting fluid) is L_w and the total length of the sections containing the less wetting fluid (called the non-wetting fluid) is L_n . The corresponding volumes are therefore given by $\pi r^2 L_w$ and $\pi r^2 L_n$, where r is the average radius of the capillary tube. The saturations

in each tube are then $S_w = L_w/L$ and $S_n = L_n/L$. Each tube making up the bundle contains the same amount of each fluid but with its own division of the fluids into bubbles.

The total volumetric flow rate q in a capillary tube at any instant of time is given by,

$$q = -\frac{\pi r^4}{8\mu_{av}L} \Theta(|\Delta P| - p_c)(|\Delta P| - p_c) \quad (4)$$

where $|\Delta P|$ is the pressure drop across the capillary tube, p_c is the instantaneous capillary pressure given by the sum of all the capillary forces along the capillary tube due to the interfaces and μ_{av} is the effective viscosity given by $\mu_{av} = S_w\mu_w + S_n\mu_n$. Here $\Theta(|\Delta P| - p_c)$ is the Heaviside function which is 0 for negative arguments and 1 for positive arguments. When the pressure difference across the tube is kept fixed, the average volumetric flow rate $\langle q \rangle$ in the steady state can be obtained by averaging Equation 4 over a time interval,

$$\langle q \rangle = -\frac{\pi r^4}{8\mu_{av}L} \text{sgn}(\Delta P) \Theta(|\Delta P| - \gamma) \sqrt{|\Delta P|^2 - \gamma^2}, \quad (5)$$

where $\text{sgn}(\Delta P)$ is the sign of the argument. If the tube is assumed to have a sinusoidal variation in radius with amplitude a about an average radius r and a period of length l , then γ is given by,

$$\gamma = \sqrt{\Gamma_s^2 + \Gamma_c^2}, \quad (6)$$

where

$$\Gamma_s = \sum_{j=-K}^{+K} \frac{4\sigma a}{r} \sin\left(\frac{\pi \Delta x_j}{l}\right) \sin\left(\frac{2\pi(x_j - x_0)}{l}\right), \quad (7)$$

and

$$\Gamma_c = \sum_{j=-K}^{+K} \frac{4\sigma a}{r} \sin\left(\frac{\pi \Delta x_j}{l}\right) \cos\left(\frac{2\pi(x_j - x_0)}{l}\right). \quad (8)$$

Here x_j is the position of center of the j th bubble if the tube is filled with $2K + 1$ bubbles. Its width is Δx_j . The surface tension times the average contact angle is σ .

We are interested in the effect due to the variation in the pore radii assuming that the average contribution due to the bubble sizes are the same for all tubes. In such a scenario, the γ can be expressed in terms of the link radius r as,

$$\gamma = \frac{k}{r} \quad (9)$$

where k is a proportionality constant. Equation 9 implies that the higher the radius of a tube, the lower the threshold pressure will be and the fluids will start flowing at a relatively lower value for $|\Delta P|$.

We now consider a bundle of N fibers with average radii drawn from a distribution $\rho(r)$. We assume there to be a smallest radius r_{\min} and a largest radius r_{\max} , so that $\rho(r) = 0$ for $r < r_{\min}$ and for $r > r_{\max}$. This means that there is a smallest threshold $P_m = k/r_{\max}$ and a largest threshold $P_M = k/r_{\min}$ among the N fibers as $N \rightarrow \infty$.

Let us define a radius

$$r_c(|\Delta P|) = \max\left(\frac{k}{|\Delta P|}, r_{\min}\right). \quad (10)$$

The total flow rate is then given by

$$\frac{Q}{N} = \begin{cases} 0 & \text{if } |\Delta P| < P_m, \\ \int_{r_c(|\Delta P|)}^{r_{\max}} q \rho(r) dr & \text{if } |\Delta P| \geq P_m, \end{cases} \quad (11)$$

which combined with Equations 9, 5 and 11 give

$$\frac{8\mu_{av}LQ}{N\pi} = \begin{cases} 0 & \text{if } |\Delta P| < P_m , \\ -\int_{r_c(|\Delta P|)}^{r_{\max}} r^4 \sqrt{|\Delta P|^2 - \left(\frac{k}{r}\right)^2} \rho(r) dr & \text{if } |\Delta P| \geq P_m . \end{cases} \quad (12)$$

2.1. Uniform distribution

We use a uniform distribution of r between $r_{\min} > 0$ and $r_{\max} > r_{\min}$ as a first illustration. We have that

$$\rho(r) = \begin{cases} 0 & \text{if } r \leq r_{\min} , \\ 1/(r_{\max} - r_{\min}) & \text{if } r_{\min} < r \leq r_{\max} , \\ 0 & \text{if } r > r_{\max} . \end{cases} \quad (13)$$

Equation 12 then gives for $|\Delta P| > k/r_{\max}$

$$Q = -\frac{k^5 N\pi}{120\mu_{av}[r_{\max} - r_c(|\Delta P|)]L} \frac{1}{|\Delta P|^4} \left[(u^2 - 1)^{3/2} (2 + 3u^2) \right]_{r_c(|\Delta P|)|\Delta P|/k}^{r_{\max}|\Delta P|/k} . \quad (14)$$

We now have two possibilities, either $|\Delta P| > k/r_{\min}$, making $r_c(|\Delta P|)|\Delta P|/k = r_{\min}|\Delta P|/k$. The other possibility is that $|\Delta P| < k/r_{\min}$ making $r_c(|\Delta P|)|\Delta P|/k = 1$.

We consider the $|\Delta P| > k/r_{\min}$ case first. This is when there is flow in all the fibers. We get

$$Q = -\frac{k^5 N\pi}{120\mu_{av}[r_{\max} - r_{\min}]L} \frac{1}{|\Delta P|^4} \left[(u^2 - 1)^{3/2} (2 + 3u^2) \right]_{r_{\min}|\Delta P|/k}^{r_{\max}|\Delta P|/k} . \quad (15)$$

For large pressure drops $|\Delta P| \gg k/r_{\min}$, this expression reduces to

$$Q = -\frac{N\pi[r_{\max}^5 - r_{\min}^5]}{40\mu_{av}[r_{\max} - r_{\min}]L} |\Delta P| . \quad (16)$$

We now consider the opposite case, i.e. when $|\Delta P| < k/r_{\min}$. In this case, $r_c(|\Delta P|)|\Delta P|/k = r_{\min}|\Delta P|/k$. The flow rate is then

$$Q = -\frac{k^5 N\pi \left[\left(\frac{r_{\max}|\Delta P|}{k} \right)^2 - 1 \right]^{3/2} \left[2 + 3 \left(\frac{r_{\max}|\Delta P|}{k} \right)^2 \right]}{120\mu_{av}[r_{\max} - k/|\Delta P|]L|\Delta P|^4} . \quad (17)$$

If we now assume that $|\Delta P| - k/r_{\max} = |\Delta P| - P_m \ll P_m$, we may expand this expression in terms of $|\Delta P| - P_m$, finding to lowest order

$$Q = -\frac{\sqrt{2} r_{\max}^{11/2} N\pi}{12\mu_{av}(r_{\max} - r_{\min})k^{1/2}L} (|\Delta P| - P_m)^{3/2} . \quad (18)$$

2.2. Power law distribution

We now consider a power law distribution where link radii are chosen with different probabilities depending on the slope of the distribution. The expression for $\rho(r)$ we assume to be

$$\rho(r) = \begin{cases} 0 & \text{if } r \leq r_{\min} , \\ \frac{1-\alpha}{r_{\max}^{1-\alpha} - r_{\min}^{1-\alpha}} r^{-\alpha} & \text{if } r_{\min} < r \leq r_{\max} , \\ 0 & \text{if } r > r_{\max} . \end{cases} \quad (19)$$

The uniform distribution (Equation 13) illustrated in the previous section is a special case of this distribution with $\alpha = 0$. The global flow rate obtained from Equation 13 is

$$Q = -\frac{k(1-\alpha)N\pi}{8\mu_{av}[r_{\max}^{1-\alpha} - r_{\min}^{1-\alpha}]L} \int_{r_c(|\Delta P|)}^{r_{\max}} r^{4-\alpha} \sqrt{\left(\frac{|\Delta P|}{k}\right)^2 - \left(\frac{1}{r}\right)^2} dr. \quad (20)$$

As for the uniform distribution, we have two cases to consider: $|\Delta P| > k/r_{\min}$ for which $r_c(|\Delta P|) = r_{\min}$ and $|\Delta P| < k/r_{\min}$ for which $r_c(|\Delta P|) = k/|\Delta P|$.

We consider the case $|\Delta P| > k/r_{\min}$ first. Then, there is flow in all the fibers and we have

$$Q = -\frac{k^{5-\alpha}(1-\alpha)N\pi}{8\mu_{av}[r_{\max}^{1-\alpha} - r_{\min}^{1-\alpha}]L|\Delta P|^{4-\alpha}} \int_{r_{\min}|\Delta P|/k}^{r_{\max}|\Delta P|/k} u^{3-\alpha} \sqrt{u^2 - 1} du. \quad (21)$$

When the pressure drop $|\Delta P|$ becomes very large, i.e., $|\Delta P| \gg k/r_{\min}$, the integral in Equation 21 simplifies by having $\sqrt{u^2 - 1} \rightarrow u$ in the integrand, and we find

$$Q = -\frac{(1-\alpha)[r_{\max}^{5-\alpha} - r_{\min}^{5-\alpha}]N\pi}{8(5-\alpha)\mu_{av}[r_{\max}^{1-\alpha} - r_{\min}^{1-\alpha}]L} |\Delta P|. \quad (22)$$

The other case, $|\Delta P| < k/r_{\min}$ leads to $r_c(|\Delta P|) = k/|\Delta P|$ and Equation 20 becomes

$$Q = -\frac{k^{5-\alpha}(1-\alpha)N\pi}{8\mu_{av}[r_{\max}^{1-\alpha} - r_{\min}^{1-\alpha}]L|\Delta P|^{4-\alpha}} \int_1^{r_{\max}|\Delta P|/k} u^{3-\alpha} \sqrt{u^2 - 1} du. \quad (23)$$

We now assume that $|\Delta P| - P_m \ll P_m$. We expand the integral in Equation 23 to find

$$\int_1^{1+\Delta} u^{3-\alpha} \sqrt{u^2 - 1} du = \int_0^\Delta (1+w)^{3-\alpha} \sqrt{2+w} \sqrt{w} dw = \frac{2\sqrt{2}}{3} \Delta^{3/2}, \quad (24)$$

to lowest order in Δ . Hence, the total flow rate is to lowest order in $|\Delta P| - P_m$

$$Q = -\frac{\sqrt{2}(1-\alpha)N\pi r_{\max}^{11/2-\alpha}}{12\sqrt{k}\mu_{av}[r_{\max}^{1-\alpha} - r_{\min}^{1-\alpha}]L} (|\Delta P| - P_m)^{3/2}. \quad (25)$$

We see that the exponent α does not affect the exponent β for $|\Delta P|$ larger than but close to P_m . Furthermore, for $\alpha = 0$ we retrieve Equation 18.

Here $P_m = k/r_{\max}$ plays the role of a threshold pressure P_c below which there is no flow, whereas $P_M = k/r_{\min}$ is the crossover pressure at which there is flow in all fibers. This pressure (P_M) signals the transition to the Darcy-type flow where Q is proportional to $|\Delta P|$.

In gist, the analytical calculations with the capillary bundle model show that as soon as the pressure drop over the fiber bundle is large enough for flow to start, it enters a non-linear regime where the total flow rate Q is proportional to $(|\Delta P| - P_m)^{3/2}$ irrespective of the exponent α , defined in Equation 19. When the threshold pressure P_M is crossed, the non-linear behavior subsides and we find Darcy-type flow. Mobility is sensitive to the details of the radius distribution for low flow rates and insensitive at higher flow rates. We like to point out here that, unlike the radii distribution, when a distribution of pore thresholds is considered, a quadratic regime with $\beta = 2$ can also be obtained for CFBM when the distribution has no lower cutoff [24]. With any non-zero lower cut-off in the thresholds, β is also 3/2 there. In the present study we considered the distribution of pore radii rather than the thresholds, and for any finite pore radii, there is always a lower cutoff in the thresholds.

3. Dynamic Pore Network Model (DPNM)

Pore-network modeling is a computational technique to simulate two-phase flow in porous media where the porous matrix is represented by a network of pores with simplified geometries. The fluid displacements inside the pores are governed by equations for fully developed flow. We use a dynamic pore-network model where the menisci positions between the fluids track the flow [29, 30]. All the pore space in this model are assigned to links and the positions where the different links meet are indicated by nodes. The flow rate in such a link is given by [28],

$$q_j = -\frac{g_j}{l_j \mu_j} \left[\Delta p_j - \sum p_c(x) \right] \quad (26)$$

where Δp_j is the local pressure drop across the j^{th} link. The terms l_j , g_j and μ_j respectively define the length, mobility and effective fluid viscosity related to that link. If μ_w and μ_n are the wetting and non-wetting viscosities respectively, then $\mu_j = s_{n,j} \mu_n + s_{w,j} \mu_w$, where $s_{n,j}$ and $s_{w,j}$ are wetting and non-wetting saturations inside that link. In this study, we consider links with circular cross sections with radii r_j , for which $g_j = a_j r_j^2 / 8$ where $a_j = \pi r_j^2$, the cross-sectional area [31]. The interfacial pressure due to surface tension between the fluids is indicated by p_c which is summed over all the interfaces inside the link j , taking into account the direction of the capillary forces. The links here represent the total pore space that consists of a pore throat in between pore bodies and the variation in the link radii along its length is therefore modeled by a sinusoidal periodic shape. The interfacial pressure at a meniscus inside such a pore can be expressed by a modified Young-Laplace equation [22],

$$|p_c(x_k)| = \frac{2\sigma \cos \theta}{r_j} \left[1 - \cos \left(\frac{2\pi x_k}{l_j} \right) \right] \quad (27)$$

where $x \in [0, l_j]$, the position of a meniscus inside the j^{th} link. Here γ and θ are the surface tension and the contact angle for the set of fluids and pores which are kept constant throughout the simulations. We considered $\sigma \cos(\theta) = 0.03\text{N/m}$ here. We study in-compressible fluids and therefore at every time step Δt we have for each node i from Kirchhoff law, $\sum q_i = 0$, where the sum is over all the links connected to i^{th} link. This, together with Equations 26 and 27 construct set of linear equations for every node. We solve these equations by conjugate gradient method [32] and determine the flow rates q_j in every link. All the menisci in each link are then advanced by an amount $\Delta x_j = q_j \Delta t$. Further technical details related to the menisci displacements can be found in [30]. We consider periodic boundary conditions that lead the system to evolve to a steady state.

The network we consider in this study consists of 64×64 links in two dimensions (2D) which form a diamond lattice. All the links are therefore at an angle 45° with respect to the overall flow direction. The links have equal lengths, $l_j = 1\text{mm}$, and the disorder appears in their radii r_j . We choose the values of r_j from a distribution $\rho(r_j)$ with a power α and in the range r_{\min} to r_{\max} given by the same type of distribution as in Equation 19,

$$\rho(r_j) = \begin{cases} 0 & \text{if } r \leq r_{\min} , \\ \frac{1-\alpha}{r_{\max}^{1-\alpha} - r_{\min}^{1-\alpha}} r_j^{-\alpha} & \text{if } r_{\min} < r \leq r_{\max} , \\ 0 & \text{if } r > r_{\max} . \end{cases} \quad (28)$$

We denote the width of the distribution by $\delta = r_{\max} - r_{\min}$. The power α generates different distribution types, $\alpha = 0$ corresponds to a uniform distribution whereas positive and negative values of α imply higher probability to find narrower and wider links respectively. Figure 1 shows $\rho(r_j)$ for $\alpha = 0.0, 1.7$ and -1.7 . For $\alpha = 0$, we show the distributions for $\delta = 0.1, 0.3$ and 0.7 .

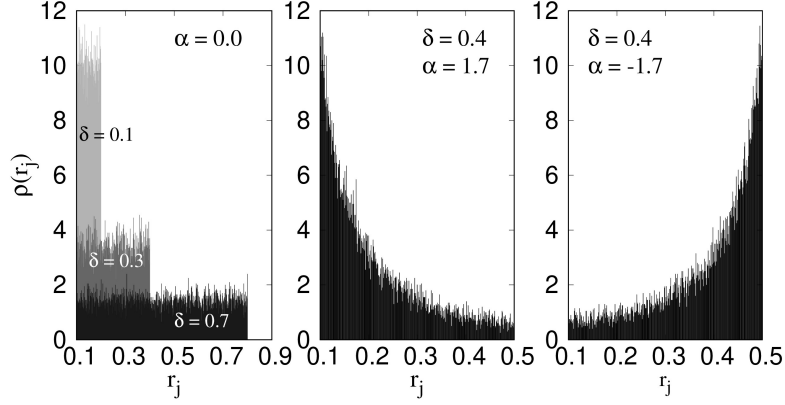


Figure 1: Distributions of link radii r_j for different values of the power α and width δ . For $\alpha = 0$ all the radii within the interval have equal probability whereas for positive and negative values of α there is higher probability to have narrow and wide links respectively.

4. Numerical results from DPNM

We perform simulations with constant global pressure drop ΔP and evolve the systems to steady states, where the macroscopic quantities fluctuate around a steady average. In the steady state, we measure the total flow rate Q . Results are averaged over 20 different samples of the pore network. By fitting the numerical data with Equation 3 for the low capillary number regime, we calculate the exponent β and the threshold pressure P_c . As there are two parameters to determine from each data set, we considered a method of minimizing the error related to the least square fit [16]. We illustrate this procedure briefly here. First we choose a trial value of β and perform least square fitting with the data points. This will provide a value of P_c and an error associated with it. We perform this for a set of β values and find the corresponding error values. We then plot the errors as a function of β . This is shown in figure 2 for five different saturations where we see non-monotonic behavior of the errors with a minimum. We then consider the value of β that corresponds to the minimum error and use the corresponding value of P_c . When plotting $\log(\Delta P - P_c)$ with $\log Q$, we find the crossover point between a non-linear and a linear regime from eye approximation. From this crossover, we then identify the crossover pressure P_t .

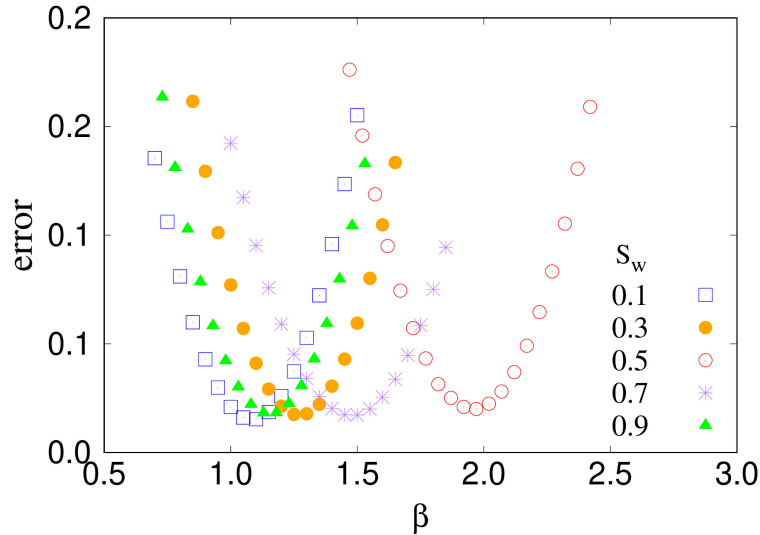


Figure 2: The error associated with least-square fitting of the numerical results to Equation 3 as a function of the trial values of β . Results are shown for five different saturations S_w . The minima of these plots decide the final values of β and P_c .

In the following we present the results showing how the steady-state rheology depends on the three parameters,

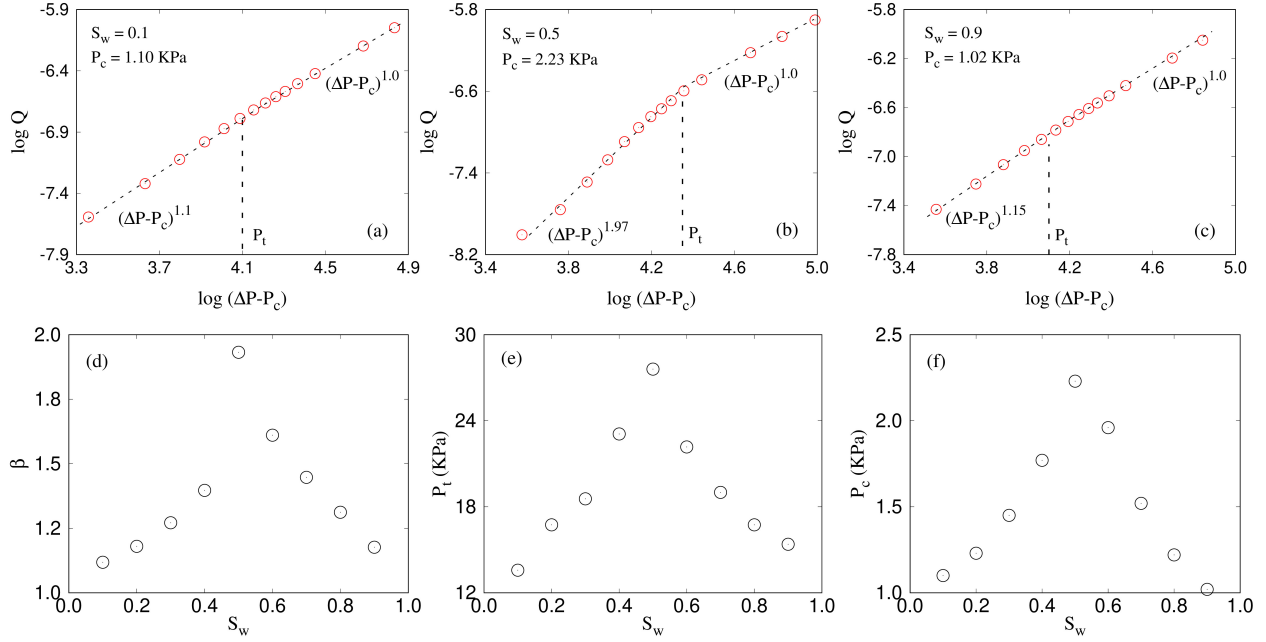


Figure 3: Plot of $\Delta P - P_c$ (Pa) vs Q (m^3/s) for a network of 64×64 links in 2D for three different wetting saturations $S_w = 0.1, 0.5$ and 0.9 are shown in (a), (b) and (c) respectively. The plots show a non-linear regime at low pressure drop and a linear regime at high pressure drop. The variations of the slopes β in the non-linear regime, the crossover pressure P_t (KPa) and the threshold pressure P_c (KPa) as a function of S_w are shown in (d), (e) and (f) respectively. All the β , P_t and P_c have a maximum around $S_w = 0.5$ and decreases on either side.

(A) the wetting saturation S_w , (B) the power α and (C) the width δ related to the pore-size distribution. We keep $r_{\min} = 0.1$ and vary r_{\max} from 0.2 to 0.8, so δ varies from 0.1 to 0.7. The exponent α is varied in the range $-1.7 \leq \alpha \leq 1.7$. We will focus on the non-linear exponent β and the pressure P_t related to the cross-over from non-linear to linear regime. In a P_t vs β plane we will then highlight how the two quantities vary when we change the values of S_w , α and δ .

4.1. Effect of S_w

The variation of the flow rate Q with the pressure drop ΔP is shown in Fig. 3 for three different wetting saturations (a) 0.1, (b) 0.5 and (c) 0.9 where we plotted $\log(Q)$ as a function of $\log(\Delta P - P_c)$. The value of α and δ are kept constant here at 0.0 and 0.3 respectively. The respective threshold pressures (P_c), measured by the minimum error method, are indicated in the plots. All the plots show a non-linear regime at lower pressure drops and then a crossover to a linear regime. However, the slope in the non-linear regime is much higher for $S_w = 0.5$ than 0.1 or 0.9. Similarly, the threshold pressure P_c is also higher for $S_w = 0.5$. This indicates the fact that as $S_w \rightarrow 0$ or $S_w \rightarrow 1$, the two-phase flow essentially approach to the single phase flow and it should eventually follow the linear Darcy law without any threshold pressure. In order to see the nature of this variation towards the linear regime, we plot in Fig. 3 (d), (e) and (f), the values of β and P_t and P_c as a function of S_w , where S_w is varied from 0.1 to 0.9 in the interval of 0.1. All three plots show a peak around $S_w = 0.5$ with $\beta = 1.97$ and then continuously decrease in both sides. The decrease in both β and P_t suggests that non only the non-linearity gradually disappears as S_w deviates from 0.5, but also the linear Darcy regime can be obtained at a relatively lower pressure drop. At the same time, the overall threshold pressure P_c also decreases as the saturation approaches to 0 or 1.

If we consider that the flow occurs in channels with capillary barriers [21], that is, the increase in Q with ΔP is contributed from two factors, the increase in the number of conducting flow paths and the increase in the flow in each path, then that explains the reduction in both β and P_t as $S_w \rightarrow 0$ or 1. As the saturation of a certain fluid decreases, either it reduces the number of fluid-fluid interfaces or produces smaller bubbles of one fluid. In both the

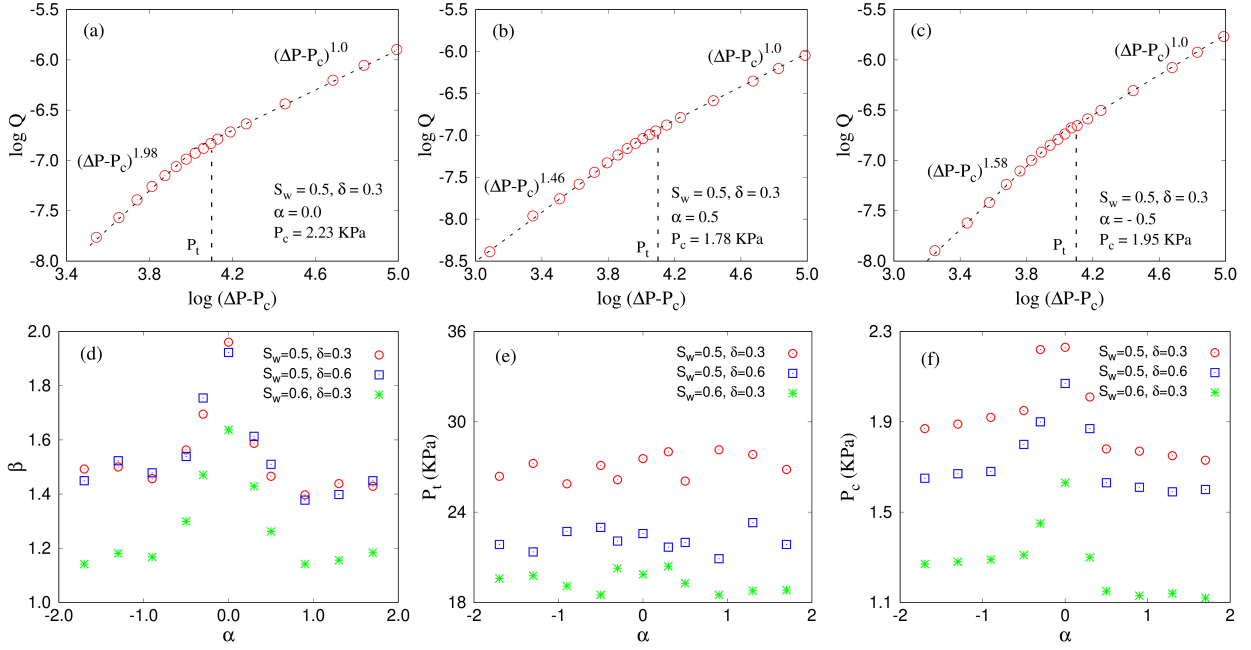


Figure 4: Variation of Q (m^3/s) as a function of $\Delta P - P_c$ (Pa) for a network of 64×64 links and for $\alpha = 0, +0.5$ and -0.5 are shown in (a), (b) and (c) respectively. The wetting saturation $S_w = 0.5$ and the distribution width $\delta = 0.3$ here. The variations of the slopes β in the non-linear regime, the crossover pressure P_t (KPa) and the threshold pressure P_c (KPa) as a function of S_w are shown in (d), (e) and (f) respectively where β has a maximum at $\alpha = 0$ whereas P_t does not show any specific dependence on α . P_c has a maximum around $\alpha = 0$ and decreases on either side.

cases the effective capillary barriers corresponding to any flow path decreases. This results in more flow paths with one fluid or with negligible capillary barriers which will start flowing as soon as any pressure drop applied, making the β to move towards 1. At the same time, the maximum capillary barrier that the model needs to overcome to make all possible paths flowing also decreases, which moves the non-linear to linear transition point to a lower value of ΔP . Experimental observation of the variation of β with saturation was first reported in [14]. No threshold pressure was considered in that study while analyzing the results in that study. A recent experimental study [20] explores the variation of β and the crossover point as a function of fractional flow, $F_w = Q_w/Q$. By balancing the surface energy to create fluid meniscus to the injection energy, they developed a theory that can predict the crossover point between the two regimes they have studied. However, they have studied the crossover from the linear regime at very low pressure drop to the non-linear regime at the intermediate pressure drop, whereas our present study addresses the crossover from the non-linear regime at the intermediate pressure drop to the linear regime at high pressure drop.

4.2. Effect of α

The power α related to the pore-size distribution function defined in Equation 28 determines the shape of the distribution and tells us how the probability of having the wider pores are compared to the narrower ones. All the pore radii within the range δ are equally probable for $\alpha = 0$ whereas positive and negative values of α indicate lower or higher probability of having wider pores respectively (Fig. 1). As the interfacial pressures are inversely proportional to r_i (Equation 27), the local capillary barriers are larger for $\alpha > 0$ compared to $\alpha < 0$. In Fig. 4 we plot $\log(\Delta P - P_c)$ with $\log(Q)$ for three different values of α , (a) 0, (b) 0.5 and (c) -0.5 . The wetting saturation and the distribution width are kept constant here at $S_w = 0.5$ and $\delta = 0.3$ respectively. A few things are to be noticed. The non-linear regime here is highly influenced by the value of α whereas the slope in linear regime remains at ≈ 1 independent of α . The exponent β is maximum for $\alpha = 0$, and then falls to 1.46 and 1.58 at $\alpha = 0.5$ and -0.5 respectively. Moreover, the threshold pressure P_c also decreases with the increase of $|\alpha|$. The decrease in P_c for

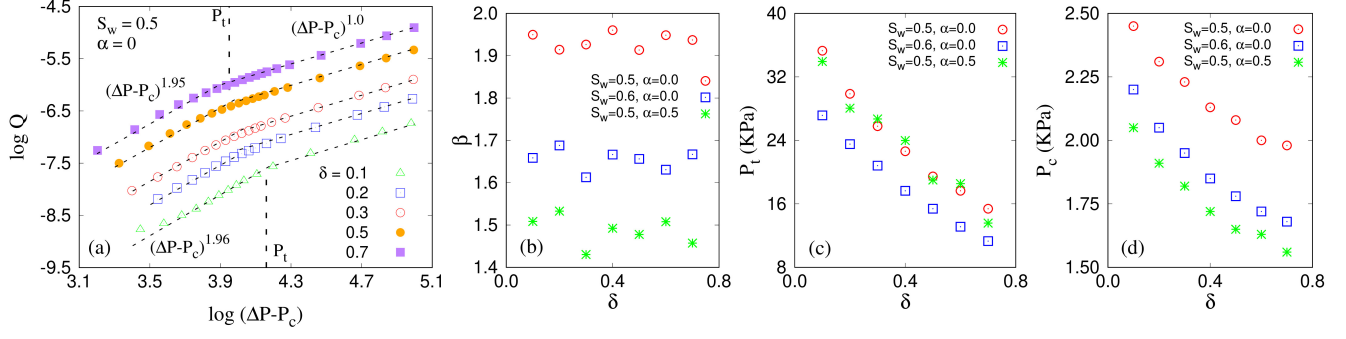


Figure 5: (a) Plot of Q (m^3/s) vs $\Delta P - P_c$ (Pa) when varying the distribution width δ where the slopes in the non-linear, as well as in the linear regimes do not show any variation with δ . In (b), (c) and (d) respectively, we show the variation of β and P_t (KPa) and P_c (KPa) with δ . In these results, α and S_w are kept constant at $\alpha = 0.0$ and $S_w = 0.5$.

$\alpha < 0$ is intuitive, since the wider pores are higher here which will cause less capillary barrier to start the flow. The decrease in P_c for $\alpha > 0$ is rather counter intuitive and may be related to the decrease in slope in the non-linear regime.

In Fig. 4 (d), we plot β as a function of α which shows the decreasing trends of β on both sides of $\alpha = 0$ and then becomes constant after it reaches to ≈ 1.5 around $|\alpha| = 1$. This indicates that any change in the fluctuations among the link radii than the uniform distribution causes slower increase in the conductive paths when increasing the ΔP . The crossover pressure P_t is plotted in Fig. 4 (e) which shows that P_t remains constant around 27KPa independent of the value or sign of α . Fig. 4 (f) shows that P_c shows a maximum at $S_w = 0.5$ and decreases on either side. The decrease of P_c for negative α is understandable as there will more links with larger radius in this case. For positive α we have less links with large radius. P_c is still observed to decrease, most probably because of the nature of the fitting since β decreases here.

Notice that, such a variation in the non-linear exponent β while varying α was not observed in case of CFBM where β has a value of $3/2$ irrespective of the radii distribution (Equation 25). This indicates that the mixing of the fluids at the nodes in a pore network has more complex effect than the flow in individual channels in CFBM. The crossover point P_t here is analogous to the maximum threshold P_M in CFBM which do not depend on α in both the models as it only depends on the span of the distribution and not on the the shape. Therefore, as we will see in the next section, P_t has a strong dependence on δ , the span of the distribution.

4.3. Effect of δ

We now perform simulations by varying the width of the radii distribution give by, $\delta = r_{\max} - r_{\min} = 0.1, 0.2, 0.3, 0.5$ and 0.7 , where r_{\min} was kept constant at 0.1 . The wetting saturation and the distribution power are kept constant here at $S_w = 0.5$ and $\alpha = 0$ respectively. The results are illustrated in Fig. 5. Interestingly, unlike the variation of β with the distribution power α as seen before, here the slopes in the non-linear regime are almost independent of the distribution width δ and remains constant around 2.0 (Fig. 5 (a)). The crossover pressure P_t , on the other hand, decreases with increase in δ , which was almost constant when we varied the distribution power α . We also found that the global threshold pressure P_c gradually decreases with increasing δ , from $P_c \approx 2.5\text{KPa}$ at $\delta = 0.1$ to $\approx 1.5\text{KPa}$ at $\delta = 0.7$. This is because as we increase δ , r_{\max} also increases and the system contains more pores with larger pore radii. This decreases the capillary barriers and hence reduces the global threshold pressure P_c .

4.4. The P_t vs β plane

To illustrate the all variations in the rheological behavior as a function of different parameters, we constructed a $P_t - \beta$ plane. This is shown in Fig. 6. We indicate all the data points there corresponding to the three sets. The

variation in the β and P_t as we increase S_w , α and δ are indicated by arrows in the plot. They can be summarized as:

Varying α : When α is increased, β decreases keeping P_t constant, and the points moves to left along a horizontal line (green squares).

Varying δ : When δ is increased, P_t decreases keeping β constant, and the points move down along a vertical line (red circles).

Varying S_w : When S_w deviates from 0.5, both β and P_t decreases and the points move to lower values along a diagonal line (purple triangles).

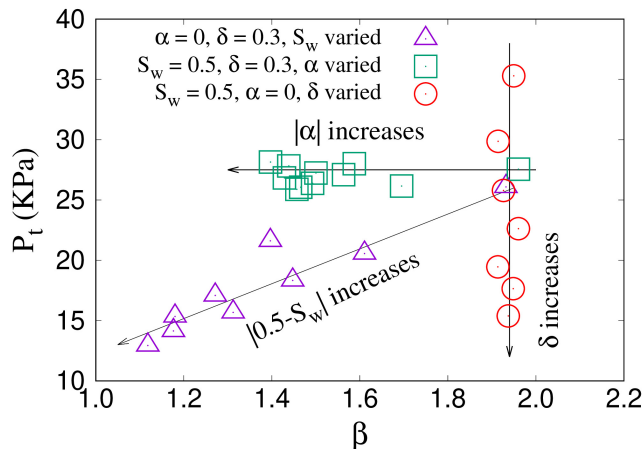


Figure 6: The $P_t - \beta$ plane, which shows the effect of varying S_w , α and δ on the rheological behavior. As S_w deviates from 0.5 (triangles), both β and P_t decreases. On the other hand, with increasing α (squares) and δ (circles) respectively, either β or P_t decreases keeping the other one constant.

5. Discussion

In this article we explored how the steady-state two-phase flow in porous media is affected by the underlying system disorder. We performed analytical calculations with a capillary bundle model and numerical simulations with dynamic pore-network model. By considering pore-radii distributions with a power α and a width δ we studied the transition from a non-linear flow regime to a linear Darcy flow. There we measured the exponent β related to the non-linear flow and cross-over pressure P_t to the linear flow. We see that the exponent β is affected by α in the dynamic network model but not in the capillary fiber bundle model. The crossover point is affected by the width δ in both models. As $|\alpha| > 0$ and we deviate from a uniform radii distribution, the slope in the non-linear regime decreases from 2 in the dynamic network model as it decreases the fluctuation in the pore-radii. On the other hand, when the width of the pore size distribution δ is increased, the linear region becomes achievable at relatively lower pressure gradient. When S_w deviates from 0.5, the two-phase flow moves closer to a single phase flow. In such circumstances, both β and P_t decreases simultaneously making the linear region more and more prominent. These numerical results can be explained qualitatively with the hypothesis that the total flow rate is contributed from the number of conducting paths and the flow in those paths [21], which makes it to increase faster than a linear behavior.

It is worth mentioning here that the single phase flow of Bingham fluid in porous media also shows similar non-linearity with a global yield threshold and a crossover to a linear regime [21, 34, 34, 35]. Nash and Rees [36] has studied Bingham fluid flow in 1d and obtained different relations between applied pressure gradient and Darcy velocity depending on the distribution of channel widths. Talon et al. [37] has analytically explored the flow of Bingham fluid in 1d channels with aperture variation and observed different scaling between pressure gradient and flow rate depending on such variation in apertures. Above studies support the fact that, when up-scaled to a certain

pore-network, both Bingham flow and two-phase flow is affected by the pore-size distribution and hence the topology of the of the network.

The effect of pore size distribution has been explored extensively in case of a single phase flow where the distribution of local fluid velocity is observed to be affected by the distribution of pore-sizes [38–42]. In the present work we demonstrated how flow equations are affected by the pore-size distribution during a two-phase flow. It will be really interesting to extend the study of velocity distribution for the two phase flow and establish a link with the flow equations through the distribution of pores.

6. Acknowledgment

This work was partly supported by the Research Council of Norway through its Centres of Excellence funding scheme, project number 262644. SS was partially supported by the National Natural Science Foundation of China under grant number 11750110430.

References

- [1] Bear, J. (1988). *Dynamics of Fluids in Porous Media*. Mineola, New York: Dover.
- [2] Dullien, F. A. L. (1992). *Porous media: Fluid, transport and pore structure*. San Diego: Academic Press.
- [3] Lenormand, R., and Zarcone, C. (1985). Invasion percolation in an etched network: measurement of a fractal dimension. *Phys. Rev. Lett.* 54, 2226. doi: 10.1103/PhysRevLett.54.2226
- [4] Chen, J. D., and Wilkinson, D. (1985). Pore-Scale Viscous Fingering in Porous Media. *Phys. Rev. Lett.* 55, 1892. doi: 10.1103/PhysRevLett.55.1892
- [5] Måløy, K. J., Feder, J., and Jøssang, T. (1985). Viscous fingering fractals in porous media. *Phys. Rev. Lett.* 55, 2688. doi: 10.1103/PhysRevLett.55.2688
- [6] Lenormand, R., Touboul, E., and Zarcone, C. (1988) Numerical models and experiments on immiscible displacements in porous media. *J. Fluid Mech.* 189, 165. doi: 10.1017/S0022112088000953
- [7] Witten, T. A. Jr., and Sander, L. M. (1981). Diffusion-limited aggregation, a kinetic critical phenomenon, *Phys. Rev. E.* 47, 1400. doi: 10.1103/PhysRevLett.47.1400
- [8] Wilkinson, D., and Willemsen, J. F. (1983). Invasion percolation: a new form of percolation theory. *J. Phys. A: Math. Gen.* 16, 3365. doi: 10.1088/0305-4470/16/14/028
- [9] Valavanides, M. (2018). Review of Steady-State Two-Phase Flow in Porous Media: Independent Variables, Universal Energy Efficiency Map, Critical Flow Conditions, Effective Characterization of Flow and Pore Network. *Transp. Porous Med.* 123, 45. doi: 10.1007/s11242-018-1026-1
- [10] Darcy, H. (1856). *Les Fontaines publiques de la ville de Dijon*. Paris: Victor Dalamont, 647.
- [11] Whitaker, S. (1986). Flow in porous media I: A theoretical derivation of Darcy’s law. *Transp. Porous Med.* 1, 3. doi: 10.1007/BF01036523
- [12] Tallakstad, K. T. , Knudsen, H. A., Ramstad, T., Løvoll, G., Måløy, K. J., Toussaint, R., and Flekkøy, E. G. (2009). Steady-state two-phase flow in porous media: Statistics and transport properties. *Phys. Rev. Lett.* 102, 074502. doi: 10.1103/PhysRevLett.102.074502

- [13] Tallakstad, K. T., Løvoll, G., Knudsen, H. A., Ramstad, T., Flekkøy, E. G., and Måløy, K. J. (2009) Steady-state, simultaneous two-phase flow in porous media: An experimental study. *Phys. Rev. E* 80, 036308. doi: 10.1103/PhysRevE.80.036308
- [14] Rassi, E. M., Codd, S. L., and Seymour, J. D. (2011). Nuclear magnetic resonance characterization of the stationary dynamics of partially saturated media during steady-state infiltration flow. *New J. Phys.* 13, 015007. doi: 10.1088/1367-2630/13/1/015007
- [15] Sinha, S., Bender, A. T., Danczyk, M., Keepseagle, K., Prather, C. A., Bray, J. M., Thrane, L. W., Seymour, J. D., Codd, S. L., and Hansen, A. (2017). Effective rheology of two-phase flow in three-dimensional porous media: experiment and simulation. *Transp. Porous Med.* 119, 77. doi: 10.1007/s11242-017-0874-4
- [16] Sinha, S., and Hansen, A. (2012). Effective rheology of immiscible two-phase flow in porous media. *Europhys. Lett.* 99, 44004. doi: 10.1209/0295-5075/99/44004
- [17] Yiotis, A. G., Talon, L., and Salin, D. (2013). Blob population dynamics during immiscible two-phase flows in reconstructed porous media. *Phys. Rev. E* 87, 033001. doi: 10.1103/PhysRevE.87.033001
- [18] Chevalier, T., Salin, D., Talon, L., and Yiotis, A. G. (2015). History effects on nonwetting fluid residuals during desaturation flow through disordered porous media. *Phys. Rev. E* 91, 043015. doi: 10.1103/PhysRevE.91.043015
- [19] Gao, Y., Lin, Q., Bijeljic, B., and Blunt, M. J. (2020). Pore-scale dynamics and the multiphase Darcy law. *Phys. Rev. Fluids*. 5, 013801. doi: 10.1103/PhysRevFluids.5.013801
- [20] Zhang, Y., Bijeljic, B., Gao, Y., Lin, Q., and Blunt, M. J. (2021). Quantification of non-linear multiphase flow in porous media. *Geophys. Res. Lett.* 48, e2020GL090477. doi: 10.1029/2020GL090477
- [21] Roux, S., and Herrmann, H. J. (1987). Disorder-induced nonlinear conductivity. *Europhys. Lett.* 4, 1227. doi: 10.1209/0295-5075/4/11/003
- [22] Sinha, S., Hansen, A., Bedeaux, D., and Kjelstrup, S. (2013). Effective rheology of bubbles moving in a capillary tube. *Phys. Rev. E* 87, 025001. doi: 10.1103/PhysRevE.87.025001
- [23] Kirkpatrick, S. (1973). Percolation and conduction. *Rev. Mod. Phys.* 45, 574. doi: 10.1103/RevModPhys.45.574
- [24] Roy, S., Hansen, A., and Sinha, S. (2019). Effective rheology of two-phase flow in a capillary fiber bundle model. *Front. Phys.* 7, 92. doi: 10.3389/fphy.2019.00092
- [25] Scheidegger, A. E. (1953). Theoretical models of porous matter, *Producers Monthly*. August 17 (1953).
- [26] Scheidegger, A. E. (1974). *The physics of flow through porous media*. Toronto: University of Toronto Press.
- [27] Hansen, A., Hemmer, P. C., and Pradhan, S. (2015). *The fiber bundle model: Modeling failure in materials*. Berlin: Wiley.
- [28] Washburn, E. W. (1921). The dynamics of capillary flow. *Phys. Rev.* 17, 273. doi: 10.1103/PhysRev.17.273
- [29] Aker, E., Maloy, K. J., Hansen, A., and Batrouni, G. G. (1998). A two-dimensional network simulator for two-phase flow in porous media. *Transp. Porous Med.* 32, 163. doi: 10.1023/A:1006510106194
- [30] Sinha, S., Gjennestad, M. Aa., Vassvik, M., and Hansen, A. (2021). Fluid meniscus algorithms for dynamic pore-network modeling of immiscible two-phase flow in porous media. *Front. Phys.* 8, 548497. doi: 10.3389/fphy.2020.548497

- [31] Langglois, W. E. (1964). *Slow Viscous Flow* New York: The Macmillan Company.
- [32] Batrouni, G. G., and Hansen, A. (1988). Fourier acceleration of iterative processes in disordered systems. *J. Stat. Phys.* 52, 747. doi: 10.1007/BF01019728
- [33] An, S., Hasan, S., Erfani, H., Babaei, M., and Niasar, V. (2020). Unravelling effects of the pore-size correlation length on the two-phase flow and solute transport properties: GPU-based pore-network modeling. *Water Resources Res.* 56, e2020WR027403. doi: 10.1029/2020WR027403
- [34] Chevalier, T., and Talon, L. (2015). Generalization of Darcys law for Bingham fluids in porous media: from flow-field statistics to the flow-rate regimes. *Phys. Rev. E.* 91, 023011. doi: 10.1103/PhysRevE.91.023011
- [35] Talon, L., and Bauer, D. (2013). On the determination of a generalized Darcy equation for yield-stress fluid in porous media using a lattice-Boltzmann TRT scheme. *Eur. Phys. J. E.* 36, 139. doi: 10.1140/epje/i2013-13139-3
- [36] Nash, S., and Rees, D. A. S. (2017). The effect of microstructure on models for the flow of a Bingham fluid in Porous media: one-dimensional flows. *Transp. Porous Med.* 116, 1073. doi:
- [37] Talon, L., Auradou, H., and Hansen, A. (2014). Effective rheology of Bingham fluids in a rough channel. *Front. Phys.* 2, 24. doi: 10.3389/fphy.2014.00024
- [38] Siena, M., Riva, M., Hyman, J. D., Winter, C. L., and Guadagnini, A. (2014). Relationship between pore size and velocity probability distributions in stochastically generated porous media. *Phys. Rev. E.* 89, 013018. doi: 10.1103/PhysRevE.89.013018
- [39] WU, A., Liu, C., Yin, S., Xue, Z., Chen, X. (2016). Pore structure and liquid flow velocity distribution in water-saturated porous media probed by MRI. *Trans. Nonferrous Met. Soc. China.* 26, 1403. doi: 10.1016/S1003-6326(16)64208-5
- [40] de Anna, P., Quaipe, B., Biro, G., and Juanes, R. (2017). Prediction of the low-velocity distribution from the pore structure in simple porous media. *Phys. Rev. Fluids.* 2, 124103. doi: 10.1103/PhysRevFluids.2.124103
- [41] Aramideh, S., Vlachos, P. P., and Ardekani, A. M. (2018). Pore-scale statistics of flow and transport through porous media. *Phys. Rev. E.* 98, 013104. doi: 10.1103/PhysRevE.98.013104
- [42] Souzy, M., Lhuissier, H., Meheust, Y., Le Borgne, T. and Metzger, B. (2020). Velocity distributions, dispersion and stretching in three-dimensional porous media. *J. Fluid Mech.* 891, A16. doi: 10.1017/jfm.2020.113